ACS APPLIED POLYMER MATERIALS

pubs.acs.org/acsapm Article

Synergistic Tetracycline–Curcumin Association in Biocompatible PCL Nanostructured Wound Dressings

Kelcilene Bruna Ricardo Teodoro,* Augusto D. Alvarenga, Paulo Augusto Marques Chagas, Raphael Guimarães Lopes, Fernanda Alves, Mirian D. Stringasci, Hilde Harb Buzzá, Natalia M. Inada, and Daniel Souza Correa*

Cite This: *ACS Appl. Polym. Mater.* 2024, 6, 5089–5101 Read Online

ACCESS | Metrics & More | Article Recommendations | Supporting Information

ABSTRACT: Open injuries, resulting from skin tissue ruptures, can expose the human body to pathogenic bacteria, presenting a significant risk for hospitalized patients and individuals with compromised immune systems. At the same time, developing alternative therapies usinginnovative methods of drug administration is crucial for combating antibacterial resistance. In this study, we present an approach for skin wound healing that synergistically combines a traditional antibiotic and an active natural compound in a polymer nanofibrous wound dressing. The fabrication strategy involved the solution blow spinning technique, which enabled easy, fast, and scalable manufacturing of polymer nanofibrous mats, while poly ε-caprolactone (PCL) was selected as the base polymer, due to its biocompatibility and nontoxicity for human tissues. The selected antibiotic formulation comprised a synergistic combination of tetracycline (TC) and curcumin (CC), aiming to incorporate reduced fractions of TC. Nanofibrous dressings measuring around 200 cm^2 could be fabricated during 45 min. The results of physicochemical characterization showed that nanofibrous mats with fewer defects were obtained due to the presence of TC in the formulation, while the presence of CC improved the encapsulation efficiency and enabled a more controlled release of TC. The antimicrobial tests demonstrated that diminishing the quantity of TC in the nanofibrous mats had no discernible impact on their efficacy against *Escherichia coli* and *Staphylococcus aureus*. The results of in vitro cytotoxicity and *in vivo* tests showed that the proposed wound dressings were not cytotoxic (cell viabilities consistently exceeded 95% for human dermal fibroblasts) and did not lead to inflammation or damage in the healing process. Moreover, the study with real wounds on mice showed that the wound dressings containing the synergistic combination of TC and CC exhibited superior efficacy in promoting healing in comparison to the control group. Collectively, these findings demonstrate the potential of the developed nanostructured platfom for wound dressing applications.

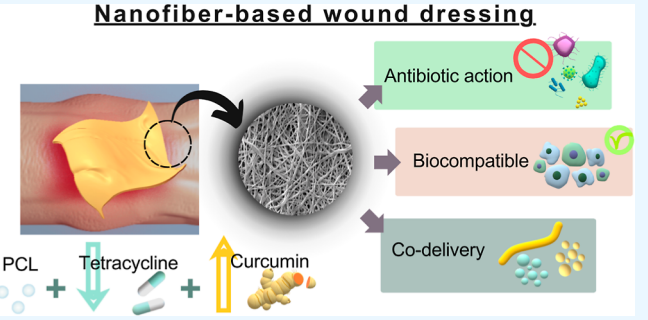

KEYWORDS: *skin wound treatments, biopolymers, biomaterial, antibiotics, solution blow spinning*

1. INTRODUCTION

Open injuries originated from skin ruptures represent a frequent concern in the medicine field.[1,2] The WHO manual on prevention and management of wound infections explains that serious infections are consequences of improperly treated wounds, such as tetanus and gas gangrene, long-term disabilities, chronic wounds, bone infections, and even death.[3] Covering the injured area with wound dressings comprises the first therapeutic intervention recommended, in order to protect the affected areas, absorb the exudates, and shorten the inflammatory process, while accelerates the healing.[2,4] Associating antimicrobial compounds with wound dressings is a beneficial strategy against the proliferation of pathogens and has been applied in many recent studies.[5−8] Moreover, discussion about the dissemination of multidrug-resistant bacterial strains indicates that, in the next 30 years, the currently known antibiotics will not be effective for treating infections, leading to an increase in the number of deaths caused by super-resistant bacteria, potentially exceeding the number of deaths from cancer or vascular diseases.[9−11] Addressing this particular challenge typically involves the development and implementation of alternative compounds, which requires significant time investment and complex steps, including the synthesis of new compounds, a deep understanding of their mechanism of action, and an assessment of potential adverse effects.[12]

Received: January 8, 2024
Revised: February 23, 2024
Accepted: March 28, 2024
Published: April 17, 2024

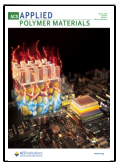

Scheme 1. Schematic Representation of (A) Injured Skin Exposed to Microorganisms and the Usual Intervention with a Common Bandage and the Topical Use of Antibiotics, (B) Compounds Used in the As-Developed Wound Dressing Fabrication: Poly(ε-caprolactone), Tetracycline Hydrochloride, and Curcumin from Saffron, (C) SBS Apparatus and the Resultant Mats, and (D) Application of Nanofibrous Dressing in Wound Healing Therapy

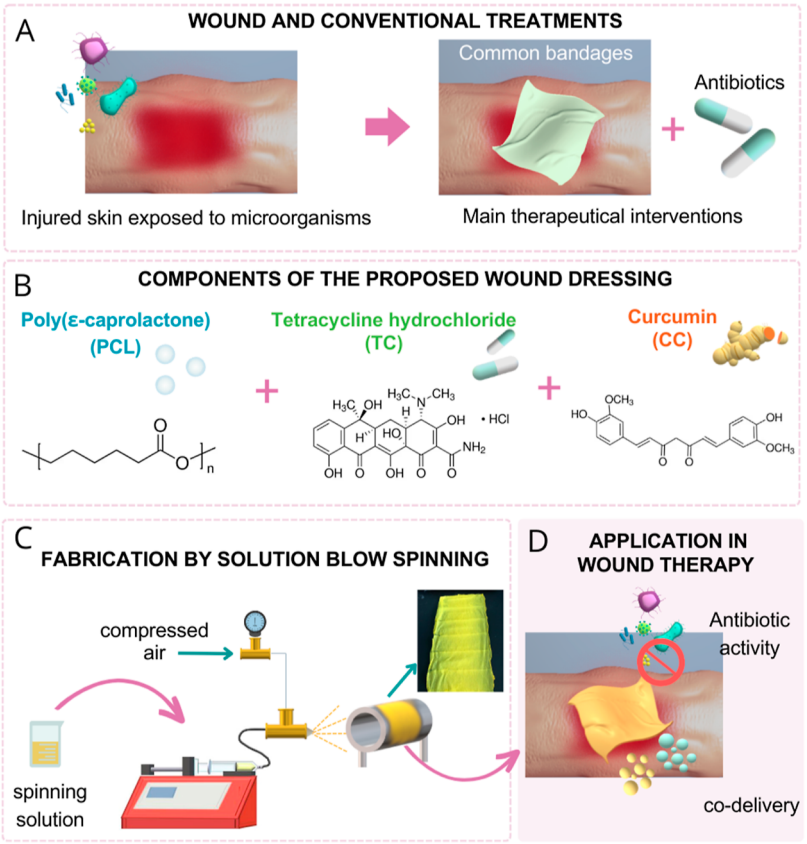

The development of effective antibacterial alternatives, as well as the synergistic combination of therapies and the use of innovative methods of administration are pointed out as important strategies for combating antimicrobial resistance.[9,11,13] In this context, the use of lower fractions of conventional drugs combined with natural compounds emerges as a suitable strategy, with some results showing antibacterial effects similar to those of conventional drugs used in an isolated way.[13−16] Among the compounds that have been tested in combination with conventional antibiotics against bacterial growth is curcumin (1,7-bis(4-hydroxy-3-methoxyphenyl)-1,6-heptadiene-3,5-dione), an active compound present in plants, known as saffron or turmeric (*Curcuma longa*).[17,18]

The strategic development of drug delivery systems also emerges as a viable solution to enhance antibiotic administration, aiming for local delivery and optimal concentration, to attenuate their concentration in healthy tissues.[16,17,19−22] Polymer nanofibers (NFs) have shown promise as drug carriers and, besides that, nanofibrous mats have exhibited properties, such as high surface area-to-volume ratio, high porosity, and similarity to the extracellular matrix, which make them very interesting substrates for wound healing applications.[22−24] The solution blow spinning (SBS) technique, illustrated in Scheme 1, allows the development of large self-standing nanofibrous mats, in a quick and reproducible way, using small amounts of reagents and a low-cost apparatus.[25,26] This technique has been shown to be suitable for the biocompatible polymer poly(ε-caprolactone) (PCL), an important material for the field of regenerative medicine and approved by the Food and Drug Administration (FDA).[26−30] While the most applied technique for nanofibrous mats for biomedical applications is electrospinning, the literature highlights the advantages of SBS due to its higher production yield, facilitating the large-scale production.

As revealed in our previous study,[26] PCL NFs produced by SBS hold significant potential for the rapid production of large nanostructured wound dressings, within a manufacturing time frame of less than 1 h, and at a low cost ($0.012 per cm^2). This study takes a step further by engineering nanostructured wound dressings using PCL through the SBS technique, which contains a reduced dosage of the conventional antibiotic tetracycline (TC) synergistically combined with the natural compound curcumin (CC). This unique combination innovates, ensuring effective antibacterial properties, while facilitating the slow release of antibiotics in minimal quantities, contributing as a strategy against the emergence of antibiotic-resistant bacterial strains, as illustrated in Scheme 1.

2. MATERIALS AND METHODS

2.1. Reagents. PCL (molar mass = 50,000 g·mol^{-1}) was acquired from Perstorp−MCassab, while chloroform, TC hydrochloride, CC, and 2,3,5-triphenyltetrazolium chloride were purchased from Sigma-Aldrich. The agar applied in microbiological essays was obtained from Kasvi and Mueller−Hinton Broth (MHB) from HiMedia. MTT (3-(4,5-dimethylthiazol-2-yl)-2,5-diphenyltetrazolium bromide) and dimethyl sulfoxide (DMSO) were purchased from Sigma-Aldrich Corp.

https://doi.org/10.1021/acsapm.4c00071
ACS Appl. Polym. Mater. 2024, 6, 5089−5101

(St. Louis, MO, USA). Fetal bovine serum and Dulbecco's modified Eagle's medium (DMEM) containing gentamicin (50 mg/L) and amphotericin B (25 μg/mL) were purchased from Vitrocell (Campinas, São Paulo, Brazil).

2.2. Wound Dressing Fabrication by SBS. The nanostructured mats were produced from PCL polymer solutions (15 wt % in chloroform) and the therapeutic compounds CC and TC were added to the PCL solution in different ratios, as specified in Table 1. These

Table 1. Theoretical TC and CC Concentrations (in Relation to the Polymer) Loaded into PCL Wound Dressings as Well as the Diameter of the NFs That Compose Them

sample name	CC (%)	TC (%)	NF diameter (nm)
PCL_	0	0	264 ± 85
PCL_TC	0	15	407 ± 135
PCL_CC	15	0	431 ± 174
PCL_2TC:1CC	7.5	7.5	485 ± 189
PCL_1TC:1CC	10	5	524 ± 165
PCL_1TC:2CC	5	10	472 ± 174
PCL_TC5	0	5	
PCL_CC10	10	0	

solutions were then processed by the SBS technique (homemade equipment available at Embrapa Instrumentation), whose apparatus, illustrated in Scheme 1, consists of a polymer solution injection system, a compressed air source, and a system for collecting the fiber mats. The injection system was composed of a 20 mL glass syringe, coupled to a capillary resistant to organic solvents, a 0.5 mm diameter nozzle, and an injection pump model NE-1010-US, One Channel 100 lb. The compressed air was supplied by a Schulz compressor, model MSV 10 VL/200−2HP, 1 stage. The air pressure was monitored using a MATHESON manometer (model 22024-1) connected to the external nozzle, which contains an internal capillary with the polymeric solution. The internal capillary was kept 2 mm away from the external nozzle, by which the compressed air flows. The rotating collector[31] was used at a speed of 180 rpm. Ambient conditions were kept uniform during the fiber processing (temperature of 25 °C and relative humidity = 35%).

2.3. Physicochemical Characterization of PCL Nanostructured Mats. The morphologies of neat and antibiotic-loaded PCL mats were investigated with scanning electron microscopy (SEM), using a JEOL (JSM-6510) microscope, operating at 5 kV. The NF diameters were estimated using ImageJ software and taking into account 100 measurements. Small pieces of each sample were attached to stubs with carbon tape and coated with gold. The chemical composition of neat and antibiotic-loaded PCL and the interaction between components were evaluated through Fourier transform infrared spectroscopy (FTIR), thermogravimetry (TGA), and differential scanning calorimetry (DSC) techniques. For FTIR analysis, a Spectrum 1000 PerkinElmer spectrometer (software Spectrum) was used, equipped with attenuated total reflection apparatus (ATR), and the spectra were obtained in absorbance mode in the range from 4000 to 400 cm^{-1}, using 32 scans and a resolution of 2 cm^{-1}. TGA was carried out with TA equipment (TGA Q500), in which the samples (10.0 ± 1 mg) were heated from room temperature until 700 °C at a heating rate of 10 °C min^{-1} and inert atmosphere (N_2—60 mL min^{-1}). TG and DTG curves were analyzed by using Origin 8 software. DSC studies were performed with a Q100 TA calorimeter. For this, samples (6.0 ± 1.0 mg) were heated from 0 to 100 °C using a heating rate of 10 °C min^{-1}, under nitrogen flow (60 mL min^{-1}). The thermograms related to the second heating of neat and loaded PCL mats were collected. Crystallinity degree was determined from the melting peak areas, using eq 1, according to Campos et al.,[32] where ΔH_m corresponds to the enthalpy of sample fusion, and ΔH_m^0 corresponds to the heat of fusion for 100% crystalline PCL (taken to be 136 J/g)[33]

$$X_c\ (\%) = \frac{\Delta H_m}{\Delta H_m^0} \times 100 \quad (1)$$

Tensile tests of the PCL nanofiber mats were carried out using dynamic mechanical analysis (DMA), using DMA Q800 equipment in thin-film tensile mode. The fibrous mats were cut with dimensions of approximately 6.74 mm in width and 5.5 mm in length, with an average thickness of 0.149 mm. The tensile test was performed in uniaxial tension with a ramp of 700 mm min^{-1}, applying a preload force of 0.001 N and deformation amplitude of 0.1% in the temperature range of 25 and 30 °C. Contact angles of PBS buffer (pH 7.4) droplets on the surface of PCL mats were measured using a contact angle measuring system (CAM 101 model KSV Instruments) equipped with a CCD camera (KGV-5000). The measures were performed using images of the angle formed between a 5 μL pipetted droplet and the surface, given that the droplet images were automatically taken as a function of time. From these images, contact angle values were calculated using dedicated software (KSV CAM 2008).

2.4. Encapsulation Efficiency and the Antibiotic In Vitro Release Assay. The CC and TC encapsulation efficiencies (EEs) were determined according to Ravikumar et al. and Göksen et al.,[34,35] using eq 2

$$\text{EE}\ (\%) = \frac{\text{amount of compound measured}}{\text{theoretical amount of compound}} \times 100 \quad (2)$$

Pieces of 6 mg of each sample were dissolved in 10 mL of chloroform under slow stirring for 12 h. After that, the absorbances were measured by using UV−vis spectroscopy. Calibration curves were prepared by dissolving TC and CC individually and in the studied proportions, using chloroform as a solvent, and measuring the main spectral bands (at 360 nm for TC and 425 nm for CC). The calibration curves and their respective equations and values of linear regression can be verified in Figure S1. All experiments were carried out in triplicate. The in vitro-controlled release assays were performed in a PBS buffer solution (0.1 mol L^{-1}, pH 7), simulating physiological conditions. Possible TC and CC degradation effects could be minimized by the addition of Tween-80 (1% in volume). Specimens of ca. 6 mg were immersed in 20 mL of the PBS/Tween-80 solution and incubated at 37 °C, protected from light, and under gentle agitation. Volumes of 500 μL were collected from each sample at a specific time interval, as described in Table S1, achieving 476 h, for monitoring the absorption bands at 360 nm for TC and 425 nm for CC, using UV−vis spectroscopy. Equal volumes of the PBS/Tween-80 solution were added after each aliquot collection in order to keep a constant volume. The experiment was performed in triplicate for each sample.

2.5. Biological Characterization. *2.5.1. Antibacterial Bioassays.* The agar diffusion assay was used to evaluate the antimicrobial activities of the wound dressings against the microorganisms *Staphylococcus aureus* (ATCC-25923) and *Escherichia coli* (ATCC-25922), in accordance with the Clinical and Laboratory Standards Institute (CLSI).[36,37] All glass materials were autoclaved at 121 °C for 20 min to ensure sterility. The experiments were carried out according to CLSI and all experiments were performed in triplicate. The bacteria were cultivated in MHB at 35 °C in an incubator for 12 h. The microorganism concentration was adjusted to 1.5×10^8 cell mL^{-1} after 12 h growth using a McFarland 0.5 scale. After that, 100 μL was pipetted on an MHB plate and spread out. Subsequently, the nanofiber mats (ϕ = 13 mm) were deposited onto an agar plate and placed in an incubator for 24 h at 35 °C. After 24 h of incubation, the inhibition zones were measured (mm) in triplicate using a Vernier caliper. The minimum inhibitory concentration (MIC) was determined using the broth microdilution method.[38] For the MIC determination, 100 μL of MBH was added to each well of a 96-well microplate. Immediately afterward, 100 μL of the tested materials was added to the first well and serial dilutions of 2 of the material were performed. Ten μL of the bacterial suspension was inoculated in each well, obtaining a final concentration of 1.5×10^8 cfu mL^{-1}. The tested concentrations of CC covered the range of

https://doi.org/10.1021/acsapm.4c00071
ACS Appl. Polym. Mater. 2024, 6, 5089−5101

1000−0.25 μg mL^{-1} and TC were 500−0.125 μg mL^{-1}. After 24 h of incubation, 20 μL of 0.5% (w/v), 2,3,5-triphenyltetrazolium chloride (TTC) solution was added to each well, and after 1 h, the color change caused by TTC was analyzed. The MIC presented was considered to be the lowest concentration where there was no visible bacterial growth.

The ability of the wound dressings to hinder the environment microbial contact with the injured skin was evaluated according to the microbial penetration test, described in detail elsewhere.[26,39,40] Specimens of 3 × 3 cm were used to seal test tubes filled with 15 mL of MHB. Negative controls (C−), referring to tubes sealed with parafilm, helped in the evaluation of asepsis of the growth medium as well as the color variations of MHB free of microorganisms. Positive controls (C+), corresponding to open test tubes (unsealed tubes), were used to evaluate variations in color and turbidity of MHB in the presence of environment microorganisms. The control and sample tubes were left exposed to the laboratory environment for 7 days. The results of this study were evaluated by visual inspection of the presence of colonies or alteration in turbidity of MHB, by deposition of 20 μL of each MHB in solid culture medium plates, and verification of the presence/absence of microorganisms after 24 h incubation.

2.5.2. Biocompatibility Evaluation. The in vitro cytotoxicity of PCL-based wound dressings was evaluated by the MTT assay,[41] following the ISO 10993-5:2009 (the International Organization for Standardization, Chapter 5: "Tests for In Vitro Cytotoxicity").[42] Following the proposal of decreasing the amount of antibiotics in wound treatments, for this analysis, the sample PCL_1TC:2 CC was chosen. For comparison purposes, extra mats containing 5 and 15% of TC (named PCL_TC5 and PCL_TC15, respectively) and containing 10% of CC (named PCL_CC10) were prepared. Specimens of all mats, measuring 1.0 ± 0.1 cm^2, were first sterilized by UVC lamp exposure of 15 min. Then, 2 pieces of 1 × 1 cm of each sample were added to a plate containing 2.5 mL of DMEM, supplemented with 10% fetal bovine serum (FBS), and kept under standard culture conditions (humidified incubator at 37 °C in a 5% CO_2 atmosphere) for 24 h to obtain the extracts that were tested in cell viability studies.

Fibroblast cell suspensions of the HDFn line (human dermal fibroblasts, neonatal, Gibco, catalog no. C0045C) from Thermo Fisher Scientific (Waltham, MA, USA) were cultivated in flasks of 75 cm^2 with DMEM supplemented with 10% FBS. At 80% confluence, cells were transferred to a 96-well plate with a density of 10^4 cells per well and maintained under standard culture conditions. After 24 h, upon reaching 80% confluence, the medium of each well was removed and replaced by 200 μL of DMEM containing the extracts of each mat and maintained for another 24 h in standard culture conditions. The medium was removed, and then the wells were washed twice with PBS before incubation with 100 μL of 0.5 mg mL^{-1} solution of MTT (3-(4,5-dimethylthiazol-2-yl)-2,5-diphenyltetrazolium bromide) for 3 h at 37 °C and 5% CO_2. The resulting formazan crystals (violet color) were solubilized in 100 μL DMSO and the resulting solution absorbance was immediately recorded in a spectrophotometer (Multiskan FC Microplate Photometer, Thermo Fisher Scientific, EUA) at 570 and 690 nm. The cell viability was expressed as a percentage of viable cells according to eq 3

$$\text{cell viability (\%)} = \frac{\text{absorbance of samples and fibroblasts}}{\text{absorbance of control}} \times 100 \quad (3)$$

The results represent the mean and standard deviation of the data normalized to controls from 12 experiments. Data were submitted to analysis of variance (ANOVA) and the means were compared by Tukey's test with a significance level of 5%, using the Origin program, version 2020 (OriginLab Corporation, Northampton, MA, USA).

2.5.3. In Vivo Test. The experimental procedures were approved by the Animal Use Ethics Committee (protocol no. 1492210521) of the São Carlos Physics Institute at the University of São Paulo, Brazil. Female Swiss mice of 6 weeks old were employed in the experiments. The animals were immunosuppressed by subcutaneous injection of prednisolone (40 mg/mL) at a dose of 100 mg/kg 1 day before the experiment. For the experiment, the animals were anesthetized with an intraperitoneal injection of ketamine (30 mg/kg) and xylazine (13 mg/kg), in addition to an intraperitoneal application of diazepam (5 mg/kg). The animals' hair was shaved in the dorsal region, and a 3 mm diameter punch was used to create a wound in the skin.

The *S. aureus* bacteria (ATCC 25923), stored at −20 °C, were reactivated on brain heart infusion (BHI) agar plates in an incubator at 37 °C for 24 h. Between 5 and 10 colonies were resuspended in a tube with 10 mL of tryptic soy broth (TSB) medium and incubated at 37 °C overnight. A 500 μL aliquot of this suspension was diluted in 9.5 mL of fresh TSB and incubated until the adjustment of optical density to 0.2 using the Varian Cary 50 UV−vis spectrophotometer (Agilent, Santa Clara, California, USA), which is equivalent to 10^8 cells per milliliter (cells/mL). From this bacterial suspension, 50 μL was applied to the wound in two applications of 25 μL with an interval of 5 min, followed by an incubation period of 15 min.

After this incubation time, the wound dressings were placed onto the wound. The region was covered with an elastic adhesive dressing (secondary dressing), which remained in place for 2 days. The following samples were tested: PCL nanostructured mat (without any other compound), only the secondary dressing, 15% CC, 10% CC, 15% TCL, 5% TCL, and one containing 10% CC + 5% TCL. Furthermore, a control group without dressing was used for comparison.

Three days after the experiment, the dressings were changed, and the animals were evaluated and euthanized with an overdose of anesthetic. Photographic images were captured with a conventional camera for qualitative analysis of each wound. Immediately before the euthanasia, microbial samples were collected using a sterile cotton swab rubbed on the wound for 30 s. After serial dilutions, the collected samples were plated on the BHI agar medium and incubated for 24 h at 37 °C. Colony-forming units were counted and evaluated for distribution and homogeneity of variance among groups. Each group was repeated with 3 animals.

3. RESULTS AND DISCUSSION

3.1. Physicochemical Characterization of SB-Spun Mats. The physical aspects of the mats (PCL and PCL_1TC_2CC, respectively), emphasizing their wide dimensions (20 cm × 10 cm), flexibility, and resistance to handling, are shown in Figure 1A,B. Figure 1 displays the SEM images of neat PCL and antibiotic-loaded PCL mats following the formulations described in Table 1. The images emphasize the nanofibrous elements that compose the wound dressing mats, and all studied conditions produced NF with diameters smaller than 500 nm, whose values are also described in Table 1. Defects such as larger diameter fibers were found in sample PCL_CC, as well as some beads and few clusters, while PCL_TC revealed a small number of larger beads. A noticeable consequence of the antibiotic incorporation is the presence of fewer imperfections in loaded NF, such as few beads and some agglomerated fibers found in samples PCL_2TC:1CC, PCL_1TC:1CC, and PCL_1TC:2CC, as well as a small variation in diameters.

The wound dressing FTIR spectra are displayed in Figure 2A. Main spectral bands are related to PCL vibration modes due to their majority in the formulation. Specifically, the PCL spectrum shows bands in three characteristic regions: starting with 1100−1600 cm^{-1},[43] representing the CO vibrations, the band at 1800−2000 cm^{-1} referring to the C═O,[43,44] in which the main peak centered at 1730 cm^{-1} is attributed to carbonyl stretching, while the band at 2300−2600 cm^{-1} refers to C−H bands.[45] The mats loaded with TC and CC FTIR spectra revealed mild significant differences since the TC and CC spectral bands can be overlapped with the PCL bands (e.g., bands in the region of 1650−1510 cm^{-1} in samples containing CC).[39,46]

https://doi.org/10.1021/acsapm.4c00071
ACS Appl. Polym. Mater. 2024, 6, 5089−5101

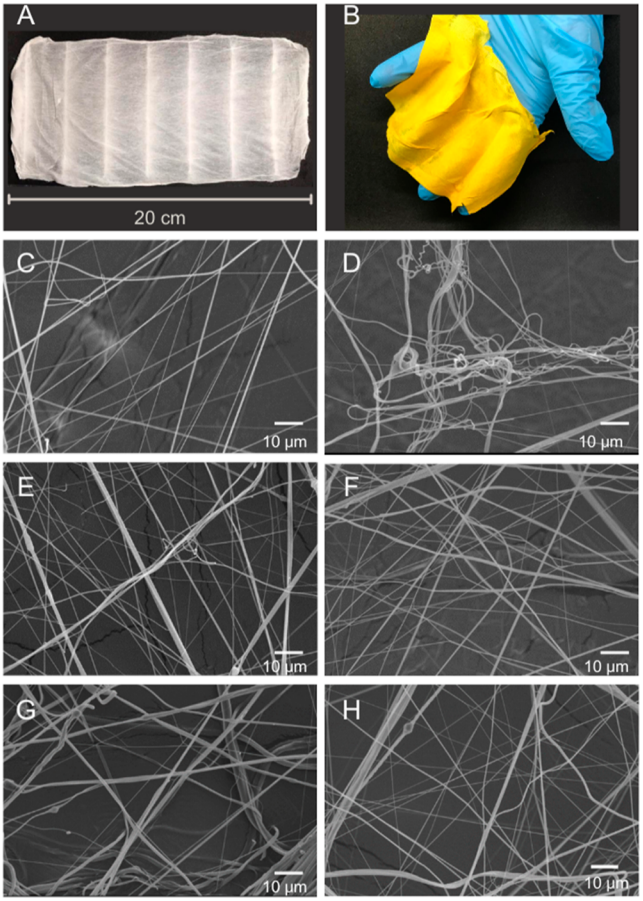

Figure 1. Digital photographs of (A) neat PCL, showing the representative size of the mats produced in this work, and (B) demonstrating the easy handling and flexibility of PLC_1TC:2CC. SEM micrographs of NFs that compose the wound dressings: (C) neat PCL, (D) PCL_2TC, (E) PCL_CC, (F) PCL_2TC:1CC, (G) PCL_1TC:1CC, and (H) PCL_1TC:2CC.

Figure 2B,C displays the TG/DTG curves for neat and loaded wound dressings. Values referring to the initial degradation temperature (T_{onset}) and ash content at 600 °C are reported in Table 2. A major event starting at around 345 °C and finishing at 470 °C is attributed to the typical profile of PCL thermal degradation under an inert atmosphere.[47,48] Minimal weight loss values at 60 °C were observed, referring to the boiling point of chloroform, indicating efficient evaporation during the production process. The thermal degradation profiles of both TC and CC were also evaluated and are shown in Figure S2 for comparative effects. Both compounds are thermally stable up to 200 °C, and the main weight loss events start around 225 °C for TC and CC, more specifically, after 205 °C for TC and 221 °C for CC, values similar to those reported previously.[49,50] The loaded PCL mats' profiles showed differences compared to neat PCL, which are related to TC and CC thermal degradation events under an inert atmosphere. For PCL_TC, an initial decline starts at around 213 °C, closer to the TC onset, and the weight loss of 4.3% occurred in the range of 200−280°. The thermal degradation profile of PCL_CC describes only a main event, which was anticipated as a result of the beginning of CC degradation, configuring the sample with the lowest T_{onset}. Samples PCL_2TC:1CC and PCL_1TC:1CC demonstrated a similar profile to the one described by PCL_TC, with the first mass loss event starting at around 211 °C, and the T_{onset} corresponding to PCL's thermal degradation profile. The PCL_1:2 sample, due to the different proportions of the components, revealed three mass loss events between 200 and 400 °C. The first one, more tenuous, starts at around 202 °C and is related to the thermal degradation of TC; the second one, more expressive than the first, starts at 250 °C and is associated with the thermal degradation of CC, whose amount is superior to TC in this sample, and the third event, corresponding to the main degradation event related to PCL, at about 348 °C. The ash content at 600 °C was high for loaded PCL mats, as a consequence of the carbonaceous residues resulting from the degradation of TC and CC under an inert atmosphere, as shown in Figure S3.

Potential interactions between the PCL matrix and the loaded compounds TC and CC were monitored by DSC analysis. Figure 2D describes the second heating curves, and the melting temperature (T_m), melting enthalpy (ΔH_m), and crystallinity index (X_c) are reported in Table 3. For all samples, a major endothermic event is observed at around 56 °C, related to the PCL melting point.[46,51] Slight changes in the endothermic peak profile are reflected in lower ΔH_m and X_c values of the loaded mats. For the T_m event, shifts in the values and shallower melting peaks are observed for the samples containing CC, which were more evident for PCL_CC and PCL_1TC:2CC. These observations suggest that this compound interferes in PCL crystallization and, as also indicated by the X_c values, these interactions did not induce PCL crystallinity. These results indicate that CC can prevent PCL interchain interactions and then impair its crystallization.[26,46] Similar effects are observed for samples loaded with TC, but at lower intensities, as corroborated by a mild shift of the melting peak and ΔH_m values.

3.1.1. Mechanical Properties and Wettability. The mechanical properties of nanofibrous mats were determined by their composition, NF diameters, and orientation of the fibers, as well as by the wound dressing thickness.[52,53] Stress−strain representative curves of solution-blown wound dressings can be verified in Figure 2E. Young's modulus values, elongation-at-break, and maximum stress-at-break are described in Table 3. All samples described a typical stress vs strain curve with the first stages referring to linear elastic behavior, followed by the plastic nonlinear region. No significant differences were observed among the samples (including neat PCL mats), as verified by the ANOVA method with at least 5% probability. Thus, all samples show the macroscopic mechanical characteristics of easy and resistant handling, required for wound dressing application.[2] Moreover, the wound dressing's mechanical resistances for handling and its flexibilities are demonstrated in Figure 1B, corroborating our previous work.[26]

Surface wettability is a parameter that must be evaluated in wound dressing applications, as it can interfere with cell adhesion and growth, as well as the absorption of exudates and drug release profile. Figure 2F shows that all samples presented a high initial contact angle, as PCL is hydrophobic due to its nonpolar nature.[54] However, the angles in the following seconds show that the incorporation of compounds led to an increase in the wettability. This is a direct consequence of TC incorporation and is more expressive for samples PCL_TC and PCL_2TC:1CC, which showed lower values at 15 s, attributed to the hydrophilic nature of TC.[47]

https://doi.org/10.1021/acsapm.4c00071
ACS Appl. Polym. Mater. 2024, 6, 5089−5101

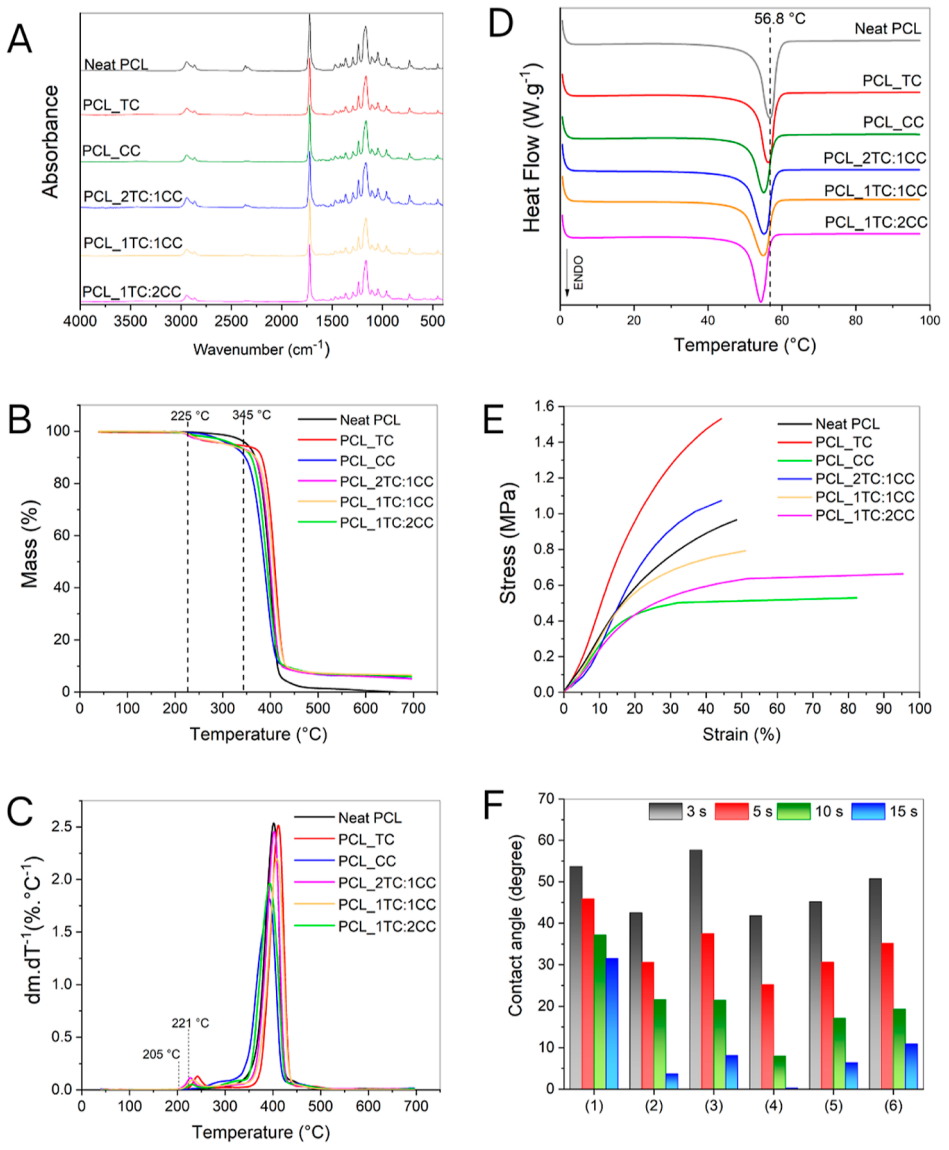

Figure 2. Physicochemical characterization of wound dressings. The compositions were analyzed from (A) FTIR spectra of PCL mats loaded with TC and CC, (B) TG and (C) DTG curves of neat and loaded PCL mats, and (D) second heating DSC curves of neat and loaded PCL mats. The mechanical performances and handling were analyzed by (E) stress−strain curves of mats obtained by the DMA tensile test and (F) the wettability was evaluated by water contact angles, where the numbers from 1 to 6 refer to neat PCL, PCL_TC, PCL_CC, PCL_2TC:1CC, PCL_1TC:1CC, and PCL_1TC:2CC, respectively.

Table 2. Onset Temperature for Wound Dressing Thermal Degradation and Ash Content at 600 °C Extracted from TG/DTG Curves for Neat and Loaded PCL Mats

sample	T_{onset} (°C)	ashes at 600°C (%)
TC	205	47.0
CC	221	34.6
neat PCL	345	0.89
PCL_TC	354	6.1
PCL_CC	329	5.9
PCL_2TC:1CC	364	5.8
PCL_1TC:2CC	348	6.6
PCL_1TC:1CC	357	6.7

3.2. Antimicrobial Performance of SB-Spun Mats. The antibacterial properties of the nanostructured PCL mats were evaluated by the agar diffusion test against the Gram-positive bacteria *S. aureus* and the Gram-negative *E. coli* as model bacterial strains.[39,55] The results of the bacterial inhibition zones are shown in Figures 3 and 4 and Table 4. While PCL is a biodegradable and biocompatible polymer, it does not exhibit antibacterial action.[56] Although the antibacterial action of CC against the bacteria *E. coli* and *S. aureus*[26,57,58] has been reported, the mats containing only CC did not show a visible inhibition halo. Physical properties such as solubility or diffusion capacity of an antimicrobial compound can hinder its diffusion on the agar medium, making a direct comparison using the agar diffusion method inappropriately.[17,26] On the other hand, all samples containing TC showed inhibition zones for *S. aureus* and *E. coli*. The wound dressings loaded uniquely with TC showed similar halo dimensions for both bacteria; however, some differences can be considered when TC is combined with CC. For *S. aureus*, the statistical analysis performed with ANOVA (α = 5%) indicated that there were no significant differences among the inhibition halos formed by the different concentrations of TC (the samples PCL and

https://doi.org/10.1021/acsapm.4c00071
ACS Appl. Polym. Mater. 2024, 6, 5089−5101

Table 3. Melting Temperature (T_m), Melting Enthalpy (ΔH_m), and Crystallinity Index (X_c) Measured by DSC and Mechanical Parameters Measured from Stress−Strain Curves Obtained by DMA Analysis for Neat and Loaded PCL Mats

sample	T_m (°C)	T_m (°C) after release	ΔH_m (J g^{-1})	ΔH_m (J g^{-1}) after release	X_c (%)	X_c (%) after release	Young's modulus (MPa)	elongation-at-break (%)	stress-at-break (MPa)
neat PCL	56.8	56.8	51.9	45.1	38.2	33.1	3 ± 0.3	51 ± 2	0.9 ± 0.08
PCL_TC	56.4	56.9	43.5	49.0	32.0	36.0	3 ± 0.6	41 ± 6	1 ± 0.2
PCL_CC	55.1	55.8	40.0	47.3	29.4	34.8	3 ± 0.3	40 ± 5	0.5 ± 0.07
PCL_2TC:1CC	55.2	55.4	46.3	48.3	34.0	35.5	2 ± 0.5	46 ± 5	0.8 ± 0.08
PCL_1TC:1CC	55.0	56.3	43.4	48.8	32.0	35.9	2 ± 0.6	50 ± 4	0.7 ± 0.08
PCL_1TC:2CC	54.3	56.1	41.4	55.1	30.4	40.5	3 ± 0.7	46 ± 7	0.7 ± 0.02

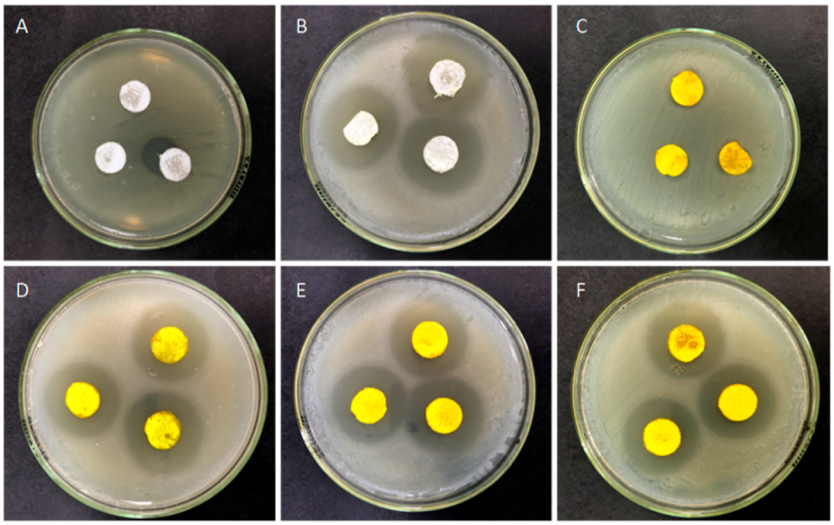

Figure 3. Inhibitory effects of the wound dressings against *S. aureus*: (A) Neat PCL, (B) PCL_TC, (C) PCL_CC, (D) PCL_2TC:1CC, (E) PCL_1TC:1CC, and (F) PCL_1TC:2CC.

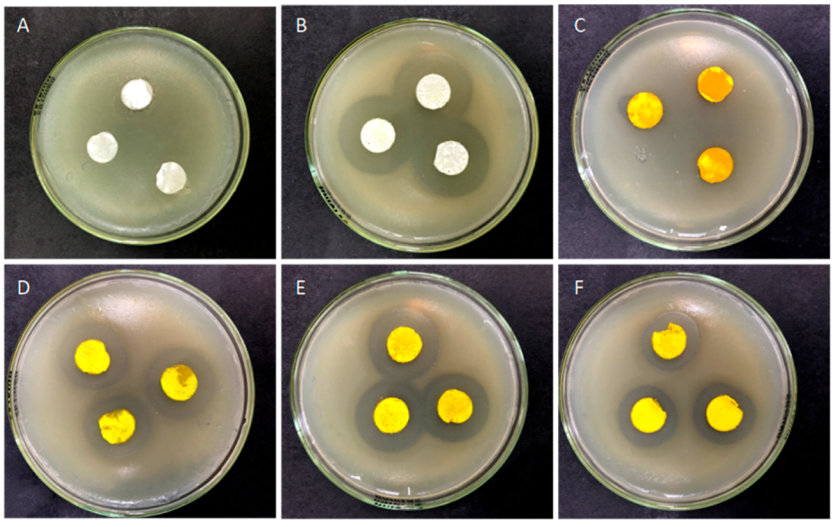

Figure 4. Inhibitory effects of the wound dressings against *E. coli*: (A) Neat PCL, (B) PCL_TC, (C) PCL_CC, (D) PCL_2TC:1CC, (E) PCL_1TC:1CC, and (F) PCL_1TC:2CC.

Table 4. Diameter (mm) of Bacterial Inhibition Zones of NFs against *S. aureus* and *E. coli*[a]

bacteria	PCL	PCL_TC	PCL_CC	PCL_2TC:1CC	PCL_1TC:1CC	PCL_1TC:2CC
S. aureus	0	32.5 ± 0.0.5	0	32.6 ± 0.5	33.0 ± 1	31.3 ± 0.5
E. coli	0	32.3 ± 0.5[a]	0	25.3 ± 0.5[b]	29.6 ± 0.5[c]	25.3 1 ± 0.5[b]

[a]Statistical analysis using the ANOVA method was applied for inhibition halo dimensions, and with Tukey's test, comparison was applied to *E. coli* data (no significant difference was verified for *S. aureus* data with at least 5% probability). The samples PCL and PCL_CC were not considered in the comparison.

https://doi.org/10.1021/acsapm.4c00071
ACS Appl. Polym. Mater. 2024, 6, 5089−5101

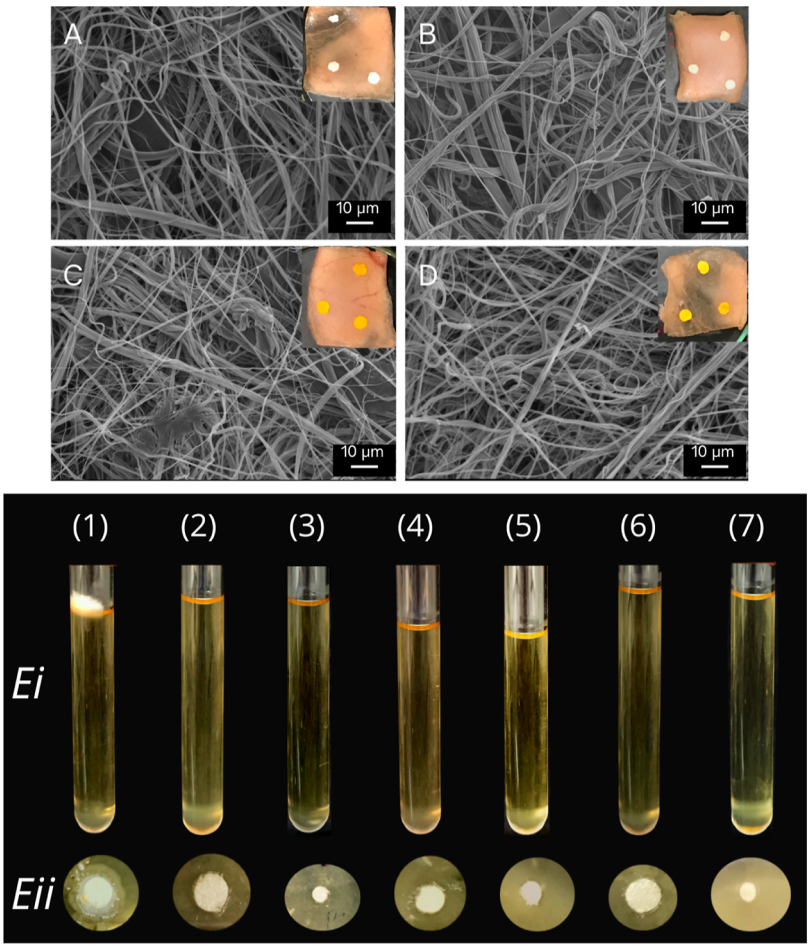

Figure 5. (A–D) Results of infected wound simulation (ex vivo): SEM images of (A) neat PCL, (B) PCL_TC, (C) PCL_CC, and (D) PCL_1TC:2CC mats after infected skin wound simulation, showing the absence of bacterial colonies adhered to the wound dressing. (A–D insets) Visual aspect of the nanofibrous mats placed onto porcine skin samples. (E) Results of microbial penetration tests: (Ei) growth/no growth of microorganisms in test tubes sealed with the respective positive (C+) (tube 1) and negative (C−) (tube 2) controls and the samples PCL_TC (tube 3), PCL_CC (tube 4), PCL_2TC:1CC (tube 5), PCL_1TC:1CC (tube 6), and PCL_1TC:2CC (tube 7) and (Eii) confirmation that there was no bacterial growth by inoculation of 20 μL of each tube matter in agar plates, followed by incubation.

Table 5. Values of TC and CC Encapsulation Efficiency of Neat and Loaded PCL Mats

sample	EE_TC (%)	EE_CC (%)
PCL_CC	0	69 ± 7
PCL_TC	57 ± 13	0
PCL_1TC:2CC	68 ± 6	60 ± 5

PCL-CC were not considered in the analysis). However, the same analysis applied to the inhibition halos formed for *E. coli* showed significant differences when the TC concentrations changed, except for the halos formed by the samples PCL_2TC:1CC and PCL_1TC:2CC. These results suggest that the additional layer present in Gram-negative bacterial membranes, which acts as a barrier against the entry of some molecules, can slightly affect the antibiotic effect of TC.[59,60] These results suggest that even the sample loaded with lower TC concentrations (PCL_1TC:2CC) can present a prominent inhibition halo. In this sense, sample PCL_1TC:2CC was chosen for the subsequent analysis.

Ex vivo assays using the porcine skin were performed to simulate a wound infected with *S. aureus*. The SEM results displayed in Figure 4A–D and visual aspects (Figure 4A–D insets) were similar to each other, characterized by the absence of the growth of *S. aureus* in the region where the PCL mats were placed. The typical grape-like *S. aureus* clusters were not found on both sides of specimens, as verified by representative SEM images shown in Figure 5A–D. The ability of the wound dressings to prevent the access of external microbes to the environment underneath the mat and protect the injured skin was also evaluated. Figure 5Ei exhibits digital photographs of test tubes filled with the MHB medium and sealed with the mats as well as the negative (C−) and positive controls (C+). Colonies are observed in C+ (Figure 5Ei—C+), which was confirmed after inoculation of 20 μL of the C+ content properly placed in sterile agar plates, as displayed in Figure 5Eii—C+. No turbidity on MHB or the presence of microorganisms was verified in the agar plate for tubes C− and for any mat, corroborating the contact inhibition observed in the aforementioned tests. In general, the results of microbiological tests demonstrated that the low hydrophilic character of PCL is suitable for the wound dressing design, as it contributes to hindering the adherence of microorganisms to the mat surfaces.

3.3. Tetracycline and Curcumin Release. Considering the theoretical concentrations described in Table 2 (totaling 15% of loaded compounds), the EE values of TC and CC for

https://doi.org/10.1021/acsapm.4c00071
ACS Appl. Polym. Mater. 2024, 6, 5089−5101

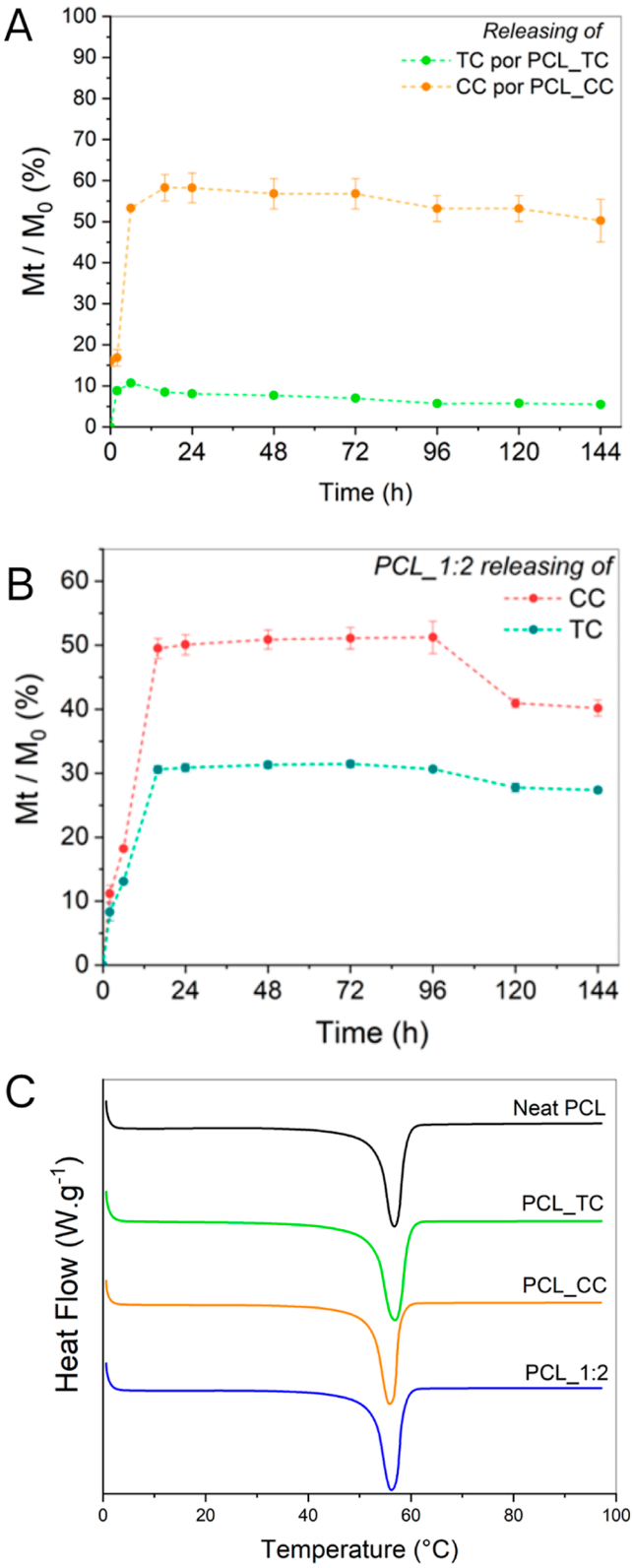

Figure 6. TC and CC curves of the cumulative release of (A) PCL_TC, PCL_CC, and (B) PCL_1TC:2CC mats during 144 h of the assay. (C) Second heating DSC curves of wound dressings after 420 h of the assay.

each sample are given in Table 5. A statistical analysis performed with the ANOVA method demonstrated no significant difference in the encapsulation of CC and TC for

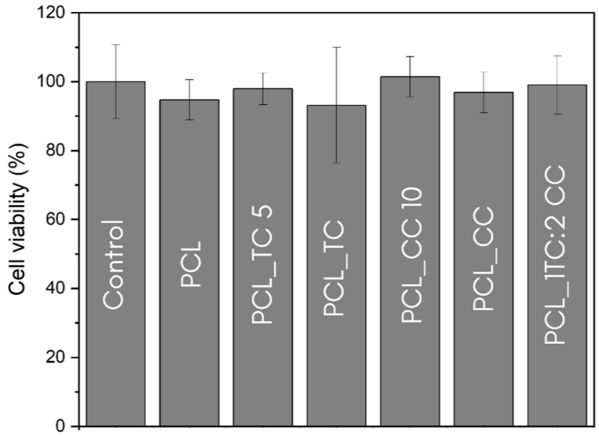

Figure 7. HDFn (human fibroblast) cell viability for wound dressings and its control samples: PCL, PCL_TC5, PCL_TC, PCL_CC10, PCL_CC, and PCL_1TC:2CC after 24 h incubation time in the presence of the extracts. Statistical analysis was performed using the one-way ANOVA method with Tukey's test comparison. No significant difference of at least 5% probability was observed in the PCL and PCL_CC groups, compared to the control group, according to Tukey's test. N = 12.

the sample PCL_1TC:2CC, compared to the control samples PCL_TC and PCL_CC, with at least 5% probability.

The co-release of TC and CC was studied by release profiles of each component separately over a period of 480 h (equivalent to 20 days). The relation between the cumulative release percentages and the time is shown in Figure 6. For the sample PCL_TC, the initial burst occurred during the first 2 h of the assay, releasing about 15% of the encapsulated content, followed by a slow and less intense release remaining until the end of the assay. As reported elsewhere,[26] for the sample containing only CC (PCL_CC), an initial burst release of about 16% is observed in the first 2 h, and a continuous release increases until the 48 h assay, followed by a cumulative release approximately constant in the range of 0−72 h. The same behavior is observed for all other samples containing CC.

The comparison of all release profiles suggests that the CC release was minimally affected by TC incorporation, except for the maximum release values. On the other hand, the release profiles described by TC, once combined with CC, showed significant differences, demonstrating the advantages of its combination with CC. Evaluating the maximum release values of each sample, one can note that the ratio 1 TC:2 CC showed an intermediary behavior between PCL_TC and PCL_CC, showing an improvement in the TC release.

The release mechanism was further investigated using four kinetic models, which can aid in inferring the phenomena involved in TC and CC release from the PCL SB-spun wound dressings. The release mechanism starts with the solubilization of the surface content of the drug, characterized by the typical bursts, and with a subsequent release of the TC and CC located more internally, associated with the diffusional process or possible erosions in the polymer structure. The kinetic models studied here were zero order,[61,62] first order,[61,63] Korsmeyer−Peppas,[64,65] and Higuchi models.[61,66] The resultant parameters calculated for each model are summarized in Table S2 for TC release and in Table S3 for CC release.

In the case of PCL_TC, the kinetic models of zero order and Korsmeyer−Peppas corresponded well to the time range of 6−72 h, suggesting, in the first case, release by leaching. In this

https://doi.org/10.1021/acsapm.4c00071
ACS Appl. Polym. Mater. 2024, 6, 5089−5101

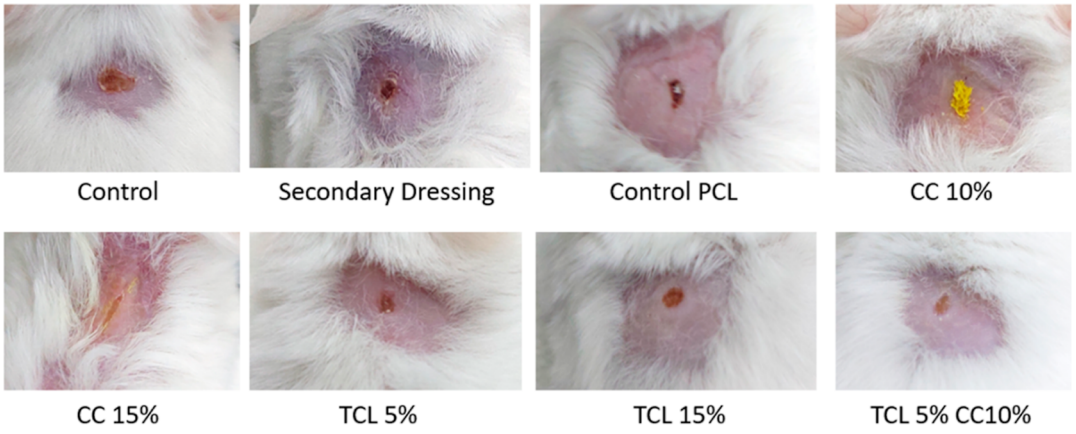

Figure 8. Images of wounds induced on the mouse skin (one animal per group) after 3 days of contact with the wound dressings. The evaluated groups were control (without any dressing), only secondary dressing, control with PCL dressing (without any treatment compound), 10% of CC, 15% of CC, 5% of TCL, 15% of TCL, and a dressing with 5% of TCL and 10% of CC.

Table 6. Number of Colony-Forming Units for Different Treatments[a]

	control	TC 5%	CC 10%	TC 5% CC 10%
log (cfu/mL)	6.88[a]	3.55[b]	6.22[a]	4.33[b]
standard deviation	0.09	0.78	0.48	1.29

[a]The indices a and b indicate the statistical difference among the treatments, according to Tukey and ANOVA tests.

case (zero-order correspondence), the release rate is independent of the TC concentration in the PCL matrix and, in the second case (Korsmeyer–Peppas correspondence), a release process is given by the combination of leaching and diffusion. For all other samples, better agreements were verified with the Korsmeyer–Peppas model. This model is widely used to represent the drug release profile of polymeric systems since it takes into account that the release occurs by more than one phenomenon.[46,64] Combining the release and DSC results, it is possible to infer that the occurrence of weak interactions between PCL and TC is responsible for the leaching behavior, while the presence of CC more interspersed between PCL chains was released both by leaching (given by its initial burst) and also by a sustained diffusional path, having a suitable correspondence with the Korsmeyer–Peppas model. Except for PCL_TC, positive kK values were found for the other samples, indicating that the presence of CC promoted a more sustained release of TC, possibly due to intermolecular interactions between TC and CC. The n values were lower than 0.5 for all samples, indicating the predominance of the typical Fickian diffusion mechanisms,[64,67] in which the release is due to the concentration gradient between the carrier (NFs) and the release media.

SEM micrographs in Figure S3 obtained after the release essay did not reveal the existence of points of degradation or scoured regions, which could indicate erosions. It supports the hypothesis of a predominantly diffusional mechanism. DSC analysis of the mats after the TC and CC release experiments showed slightly lower X_c values for pure PCL, suggesting the occurrence of a certain level of degradation. The other samples showed higher X_c values, similar to the pure PCL (after processing and before release), and narrower and deeper PCL melting peaks, indicating the removal of components that interfere with PCL crystallization.

3.4. Biocompatible Evaluation: In Vitro Cytotoxicity and In Vivo Tests. The cytotoxicity of the proposed PCL_1TC:2CC mats was investigated toward neonatal human dermal fibroblast (HDFn) cells. For this purpose, the cells were cultured in extracts prepared from PCL_1TC:2CC and control samples containing different concentrations of each compound: neat PCL, PCL_TC, PCL_CC, PCL_TC5, and PCL_CC10. The samples were submitted to the MTT viability assay (Figure 7), in which the HDFn cells were exposed for 24 h at physiological conditions (37 °C and 5% CO_2), in the presence of the different mat's extracts, obtained after 24 h incubation in DMEM plus 10% FBS. The evaluation of the results followed the ISO 10993-5,[68] (qualitative morphological grading of the cytotoxicity of extracts), and for all samples, the averages of HDFn cell viability were above 95%. These results indicate that no cytotoxicity to human fibroblasts was verified for the compounds extracted from the proposed wound dressings.

In vivo tests regarding the different treatments were carried out on wounds induced on the mouse skin. In Figure 8, it is possible to observe the appearance of the lesions 72 h after treatment, in which all treatment groups (secondary dressing, control PCL, CC 10%, CC 15%, TCL 5%, TCL 15%, and TCL 5% CC 10%) present more healed wounds in relation to the control group (no treatment was performed). Furthermore, for the TCL 5% CC 10% group, none of the animals showed inflammation or any other indication of worsening healing compared to the TCL 5% and TCL 15% groups.

After 72 h of treatment, microbial samples were also collected using a sterile cotton swab rubbed on the wound. Colony-forming units were counted after 24 h and the results are presented in Table 6.

The CC 10% group was similar to the control group, where 6.22 log of the bacteria was recovered, probably due to the low diffusion of the molecule when not associated with TC. The TC 5% group reduced 3.55 log of the bacteria, reaching a reduction equivalent to 3.33 log compared to the control. The TC 5% CC 10% group recovered 4.33 logs, which corresponds to a reduction of 2.55 logs of *S. aureus* bacteria. Both TC 5% and TC 5% CC 10% groups were statistically different from the control group and similar to each other. In summary, our results indicate that the groups of mice treated with TC 5% and TC 5% CC 10% demonstrated the most effective

https://doi.org/10.1021/acsapm.4c00071
ACS Appl. Polym. Mater. 2024, 6, 5089−5101

inactivation capability values compared to the control group, corroborating their potential for wound dressing applications.

4. CONCLUSIONS

In this study, we successfully developed a biocompatible nanofibrous wound dressing that contains the synergistic combination of TC and CC, aiming to promote enhanced skin wound healing. The integration of PCL nanofibers with the synergistic antibiotic formulation, using the SBS technique, aimed to achieve a cost-effective and rapid manufacturing process for wound dressings. The SBS technique met the criteria for fast wound dressing fabrication, resulting in large dressings with appropriate mechanical resistance, ease of handling, optimal wettability, and protection against environmental microorganisms. Additionally, the proposed wound dressings were capable of releasing CC and TC, leading to a pronounced antibiotic effect. Microbiological assessments indicated that the antibacterial effect of TC persisted even when fractionated and combined with CC. Besides, the fibrous mats have demonstrated efficacy against microbial adhesion and penetration from the external environment. Notably, the presence of CC played a pivotal role in achieving a sustained co-release profile for both components, with the sample PCL_1TC:2CC (containing the lower fraction of conventional antibiotic) reaching a maximum release of 60% of the CC content and 68% of the TC content at 72 h. Importantly, the extracts released from the wound dressings showed no cytotoxicity for human dermal fibroblasts, reaching with cell viabilities above 95%. Ultimately, in vivo tests conducted on induced wounds in mice skin demonstrated that the mats promoted effective healing, with an absence of inflammation. These findings demonstrate the potential of our developed nanostructured platform for wound healing applications.

■ ASSOCIATED CONTENT

Supporting Information

The Supporting Information is available free of charge at https://pubs.acs.org/doi/10.1021/acsapm.4c00071.

Calibration curves used to calculate the EE of TC and CC; data related to the collection of experimental data from the release assay; TGA and dTG curves of TC and CC; constants and coefficient of correlation (R^2) for different mathematical models applied to TC and CC release; and representative SEM images of the wound dressings after controlled release study (PDF)

■ AUTHOR INFORMATION

Corresponding Authors

Kelcilene Bruna Ricardo Teodoro − *Nanotechnology National Laboratory for Agriculture (LNNA), Embrapa Instrumentação, 13560-970 São Carlos, São Paulo, Brazil;* orcid.org/0000-0003-4337-4849; Email: kbr.teodoro@gmail.com

Daniel Souza Correa − *Nanotechnology National Laboratory for Agriculture (LNNA), Embrapa Instrumentação, 13560-970 São Carlos, São Paulo, Brazil;* orcid.org/0000-0002-5592-0627; Email: daniel.correa@embrapa.br

Authors

Augusto D. Alvarenga − *Nanotechnology National Laboratory for Agriculture (LNNA), Embrapa Instrumentação, 13560-970 São Carlos, São Paulo, Brazil;* orcid.org/0000-0002-0996-8785

Paulo Augusto Marques Chagas − *Nanotechnology National Laboratory for Agriculture (LNNA), Embrapa Instrumentação, 13560-970 São Carlos, São Paulo, Brazil;* orcid.org/0000-0002-1399-4054

Raphael Guimarães Lopes − *São Carlos Institute of Physics, University of São Paulo, 13566-590 São Carlos, São Paulo, Brazil*

Fernanda Alves − *São Carlos Institute of Physics, University of São Paulo, 13566-590 São Carlos, São Paulo, Brazil*

Mirian D. Stringasci − *São Carlos Institute of Physics, University of São Paulo, 13566-590 São Carlos, São Paulo, Brazil*

Hilde Harb Buzzá − *Institute of Physics, Pontificia Universidad Católica de Chile, 7820436 Santiago, Chile*

Natalia M. Inada − *São Carlos Institute of Physics, University of São Paulo, 13566-590 São Carlos, São Paulo, Brazil*

Complete contact information is available at: https://pubs.acs.org/10.1021/acsapm.4c00071

Notes

The authors declare no competing financial interest.

■ ACKNOWLEDGMENTS

The authors thank the financial support from the Conselho Nacional de Desenvolvimento Científico e Tecnológico (CNPq) (382244/2020-6, 381405/2021-4), Fundação de Amparo à Pesquisa do Estado de São Paulo (FAPESP) (2013/07276-1, 2018/22214-6, 2023/13428-0), MCTI-SisNano, Coordenação de Aperfeiçoamento de Pessoal de Nível Superior, Brasil (CAPES) (financing code 001), and Rede Agronano-EMBRAPA from Brazil.

■ REFERENCES

(1) Ambekar, R. S.; Kandasubramanian, B. Advancements in Nanofibers for Wound Dressing: A Review. *Eur. Polym. J.* **2019**, *117* (May), 304−336.

(2) Teodoro, K. B. R.; Santos, D. M.; Ballesteros, C. A. S.; Chagas, P. A. M.; Costa, V. P. V.; Schneider, R.; Correa, D. S. Multifunctional Wound Dressings Based on Electrospun Nanofibers. *Electrospun Nanofibers*; Springer International Publishing: Cham, 2022; pp 297−329.

(3) World Health Organization. *Prevention and Management of Wound Infection*, 2013; pp 1−3.

(4) Sharifi, S.; Hajipour, M. J.; Gould, L.; Mahmoudi, M. Nanomedicine in Healing Chronic Wounds: Opportunities and Challenges. *Mol. Pharmaceutics* **2021**, *18* (2), 550−575.

(5) Wang, Y.; Wang, X.; Zhou, D.; Xia, X.; Zhou, H.; Wang, Y.; Ke, H. Preparation and Characterization of Polycaprolactone (PCL) Antimicrobial Wound Dressing Loaded with Pomegranate Peel Extract. *ACS Omega* **2023**, *8* (23), 20323−20331.

(6) Wang, W.; Jia, B.; Xu, H.; Li, Z.; Qiao, L.; Zhao, Y.; Huang, H.; Zhao, X.; Guo, B. Multiple Bonds Crosslinked Antibacterial, Conductive and Antioxidant Hydrogel Adhesives with High Stretchability and Rapid Self-Healing for MRSA Infected Motion Skin Wound Healing. *Chem. Eng. J.* **2023**, *468*, 143362.

(7) Jia, B.; Li, G.; Cao, E.; Luo, J.; Zhao, X.; Huang, H. Recent Progress of Antibacterial Hydrogels in Wound Dressings. *Mater. Today Bio* **2023**, *19*, 100582.

(8) Huang, H.; Dong, Z.; Ren, X.; Jia, B.; Li, G.; Zhou, S.; Zhao, X.; Wang, W. High-Strength Hydrogels: Fabrication, Reinforcement Mechanisms, and Applications. *Nano Res.* **2023**, *16* (2), 3475−3515.

(9) Wencewicz, T. A. Crossroads of Antibiotic Resistance and Biosynthesis. *J. Mol. Biol.* **2019**, *431* (18), 3370−3399.

(10) Stokes, J. M.; Lopatkin, A. J.; Lobritz, M. A.; Collins, J. J. Bacterial Metabolism and Antibiotic Efficacy. *Cell Metab.* **2019**, *30* (2), 251−259.
(11) Vivas, R.; Barbosa, A. A. T.; Dolabela, S. S.; Jain, S. Multidrug-Resistant Bacteria and Alternative Methods to Control Them: An Overview. *Microb. Drug Resist.* **2019**, *25* (6), 890−908.
(12) Qin, H. L.; Zhang, Z. W.; Ravindar, L.; Rakesh, K. P. Antibacterial Activities with the Structure-Activity Relationship of Coumarin Derivatives. *Eur. J. Med. Chem.* **2020**, *207*, 112832.
(13) Ayaz, M.; Ullah, F.; Sadiq, A.; Ullah, F.; Ovais, M.; Ahmed, J.; Devkota, H. P. Synergistic Interactions of Phytochemicals with Antimicrobial Agents: Potential Strategy to Counteract Drug Resistance. *Chem. Biol. Interact.* **2019**, *308* (May), 294−303.
(14) Langeveld, W. T.; Veldhuizen, E. J. A.; Burt, S. A. Synergy between Essential Oil Components and Antibiotics: A Review. *Crit. Rev. Microbiol.* **2014**, *40* (1), 76−94.
(15) Yulinah Su, E.; Fisheri Ku, N.; Puspatrian, K.; Puspita Ad, H. Antibacterial Activity of Curcumin in Combination with Tetracycline Against Staphylococcus Aureus by Disruption of Cell Wall. *Res. J. Med. Plants* **2018**, *12* (1), 1−8.
(16) Lin, Z.; Tsai, T.; Yu, K.; Nien, Y.; Liu, R.; Liu, G.; Chi, P.; Fang, Y.; Ko, B.; Law, W.; Zhou, C.; Yong, K.; Cheng, P.; Chen, C. Creation of Chitosan-Based Nanocapsule-in-Nanofiber Structures for Hydrophobic/Hydrophilic Drug Co-Delivery and Their Dressing Applications in Diabetic Wounds. *Macromol. Biosci.* **2023**, *23*, 2300145.
(17) Chakravorty, A.; Biswas, B.; Sankar Sana, S.; Rayan, R. A.; Lala, N. L.; Ramakrishna, S. A Review on Toxicity of Turmeric Derived Nano-Formulates against Bacterial and Fungal Cells with Special Emphasis on Electrospun Nanofibers. *Mater. Today: Proc.* **2021**, *46*, 6358−6362.
(18) Wulandari, A.; Sunarti, T. C.; Fahma, F.; Enomae, T. The Potential of Bioactives as Biosensors for Detection of PH. *IOP Conf. Ser. Earth Environ. Sci.* **2020**, *460* (1), 012034.
(19) Fereydouni, N.; Darroudi, M.; Movaffagh, J.; Shahroodi, A.; Butler, A. E.; Ganjali, S.; Sahebkar, A. Curcumin Nanofibers for the Purpose of Wound Healing. *J. Cell. Physiol.* **2019**, *234* (5), 5537−5554.
(20) Awan, J. A.; Rehman, S. U.; Bangash, M. K.; Ali, U.; Asad, M.; Hussain, F.; Jaubert, J.-N. Development and Characterization of Electrospun Curcumin-Loaded Antimicrobial Nanofibrous Membranes. *Text. Res. J.* **2020**, *91*, 1478−1485.
(21) Gutierrez-Gonzalez, J.; Garcia-Cela, E.; Magan, N.; Rahatekar, S. S. Electrospinning Alginate/Polyethylene Oxide and Curcumin Composite Nanofibers. *Mater. Lett.* **2020**, *270*, 127662.
(22) Akrami-Hasan-Kohal, M.; Tayebi, L.; Ghorbani, M. Curcumin-Loaded Naturally-Based Nanofibers as Active Wound Dressing Mats: Morphology, Drug Release, Cell Proliferation, and Cell Adhesion Studies. *New J. Chem.* **2020**, *44* (25), 10343−10351.
(23) Chan Park, S.; Kim, M. J.; Choi, K.; Kim, J.; Choi, S. O. Influence of Shell Compositions of Solution Blown PVP/PCL Core-Shell Fibers on Drug Release and Cell Growth. *RSC Adv.* **2018**, *8* (57), 32470−32480.
(24) Kharaghani, D.; Gitigard, P.; Ohtani, H.; Kim, K. O.; Ullah, S.; Saito, Y.; Khan, M. Q.; Kim, I. S. Design and Characterization of Dual Drug Delivery Based on In-Situ Assembled PVA/PAN Core-Shell Nanofibers for Wound Dressing Application. *Sci. Rep.* **2019**, *9* (1), 12640.
(25) Liu, F.; Saricaoglu, F. T.; Avena-Bustillos, R. J.; Bridges, D. F.; Takeoka, G. R.; Wu, V. C. H.; Chiou, B. S.; Wood, D. F.; McHugh, T. H.; Zhong, F. Antimicrobial Carvacrol in Solution Blow-Spun Fish-Skin Gelatin Nanofibers. *J. Food Sci.* **2018**, *83* (4), 984−991.
(26) Teodoro, K. B. R.; Alvarenga, A. D.; Rocha Oliveira, L. F.; Marques Chagas, P. A.; Lopes, R. G.; Andre, R. d. S.; Mercante, L. A.; Alves, F.; Stringasci, M. D.; Buzza, H. H.; Inada, N. M.; Correa, D. S. Fast Fabrication of Multifunctional PCL/Curcumin Nanofibrous Membranes for Wound Dressings. *ACS Appl. Bio Mater.* **2023**, *6* (6), 2325−2337.
(27) Dash, T. K.; Konkimalla, V. B. Poly-ϵ-caprolactone based formulations for drug delivery and tissue engineering: A review. *J. Controlled Release* **2012**, *158* (1), 15−33.
(28) Nagrath, M.; Sikora, A.; Graca, J.; Chinnici, J. L.; Rahman, S. U.; Reddy, S. G.; Ponnusamy, S.; Maddi, A.; Arany, P. R. Functionalized Prosthetic Interfaces Using 3D Printing: Generating Infection-Neutralizing Prosthesis in Dentistry. *Mater. Today Commun.* **2018**, *15*, 114−119.
(29) Shen, C.; Wu, M.; Sun, C.; Li, J.; Wu, D.; Sun, C.; He, Y.; Chen, K. Chitosan/PCL nanofibrous films developed by SBS to encapsulate thymol/HPβCD inclusion complexes for fruit packaging. *Carbohydr. Polym.* **2022**, *286*, 119267.
(30) Shen, X.; Zheng, L.; Tang, R.; Nie, K.; Wang, Z.; Jin, C.; Sun, Q. Double-Network Hierarchical-Porous Piezoresistive Nanocomposite Hydrogel Sensors Based on Compressive Cellulosic Hydrogels Deposited with Silver Nanoparticles. *ACS Sustain. Chem. Eng.* **2020**, *8* (19), 7480−7488.
(31) Alvarenga, A. D. S.; Correa, D. Coletor vazado de hastes rotativo para coleta e secagem rápida de micronanofibras produzidas pelo método de fiação por sopro em solução (SBS); **2020**.
(32) Campos, A.; Teodoro, K. B. R.; Teixeira, E. M.; Corrêa, A.; Marconcini, J. M.; Wood, D. F.; Williams, T. G.; Mattoso, L. H. C. Properties of Thermoplastic Starch and TPS/Polycaprolactone Blend Reinforced with Sisal Whiskers Using Extrusion Processing. *Polym. Eng. Sci.* **2013**, *53* (4), 800−808.
(33) De Kesel, C.; Lefèvre, C.; Nagy, J. B.; David, C. Blends of Polycaprolactone with Polyvinylalcohol: A DSC, Optical Microscopy and Solid State NMR Study. *Polymer* **1999**, *40* (8), 1969−1978.
(34) Ravikumar, R.; Ganesh, M.; Ubaidulla, U.; Young Choi, E.; Tae Jang, H. Preparation, Characterization, and in Vitro Diffusion Study of Nonwoven Electrospun Nanofiber of Curcumin-Loaded Cellulose Acetate Phthalate Polymer. *Saudi Pharm. J.* **2017**, *25* (6), 921−926.
(35) Göksen, G.; Fabra, M. J.; Ekiz, H. I.; López-Rubio, A. Phytochemical-Loaded Electrospun Nanofibers as Novel Active Edible Films: Characterization and Antibacterial Efficiency in Cheese Slices. *Food Control* **2020**, *112*, 107133.
(36) CLSI Clinical and Laboratory Standards Institute. *Performance Standards for Antimicrobial Susceptibility Testing; Fifteenth Informational Supplement. CLSI/NCCLS Document M100-S15*: USA, 2005; p 19087.
(37) Clinical and Laboratory Standards Institute. *No TitleCLSI. M26-A: Methods for Determining Bactericidal Activity of Antimicrobial Agents; Approved Guideline*: USA, 1999; pp 13−15.
(38) Tenover, F. C. Antibiotic Susceptibility Testing. *Encyclopedia of Microbiology*; Elsevier, 2009; pp 67−77.
(39) Chagas, P. A. M.; Schneider, R.; dos Santos, D. M.; Otuka, A. J. G.; Mendonça, C. R.; Correa, D. S. Bilayered Electrospun Membranes Composed of Poly(Lactic-Acid)/Natural Rubber: A Strategy against Curcumin Photodegradation for Wound Dressing Application. *React. Funct. Polym.* **2021**, *163*, 104889.
(40) Tang, Y.; Zhou, Y.; Lan, X.; Huang, D.; Luo, T.; Ji, J.; Mafang, Z.; Miao, X.; Wang, H.; Wang, W. Electrospun Gelatin Nanofibers Encapsulated with Peppermint and Chamomile Essential Oils as Potential Edible Packaging. *J. Agric. Food Chem.* **2019**, *67* (8), 2227−2234.
(41) Wu, C.-S.; Hsu, Y.-C.; Liao, H.-T.; Cai, Y.-X. Antibacterial Activity and in Vitro Evaluation of the Biocompatibility of Chitosan-Based Polysaccharide/Polyester Membranes. *Carbohydr. Polym.* **2015**, *134*, 438−447.
(42) International Organization for Standardization. *Biological Evaluation of Medical Devices—Part 5: Tests for in Vitro Cytotoxicity—ISO 10993-5:2009(E)*, 2009; p 572.
(43) Li, R.; Li, Z.; Yang, R.; Yin, X.; Lv, J.; Zhu, L.; Yang, R. Polycaprolactone/Poly(L-Lactic Acid) Composite Micro/Nanofibrous Membrane Prepared through Solution Blow Spinning for Oil Adsorption. *Mater. Chem. Phys.* **2020**, *241*, 122338.
(44) Lorente, M. A.; Corral, A.; González-Benito, J. PCL/Collagen Blends Prepared by Solution Blow Spinning as Potential Materials for Skin Regeneration. *J. Appl. Polym. Sci.* **2021**, *138* (21), 50493.

https://doi.org/10.1021/acsapm.4c00071
ACS Appl. Polym. Mater. 2024, 6, 5089−5101

(45) Cao, Y.; Shen, C.; Yang, Z.; Cai, Z.; Deng, Z.; Wu, D. Polycaprolactone/Polyvinyl Pyrrolidone Nanofibers Developed by Solution Blow Spinning for Encapsulation of Chlorogenic Acid. *Food Qual. Saf.* **2022**, *6*, fyac014.
(46) Sharma, D.; Satapathy, B. K. Understanding Release Kinetics and Collapse Proof Suture Retention Response of Curcumin Loaded Electrospun Mats Based on Aliphatic Polyesters and Their Blends. *J. Mech. Behav. Biomed. Mater.* **2021**, *120*, 104556.
(47) Dias, A. M.; da Silva, F. G.; Monteiro, A. P. d. F.; Pinzón-García, A. D.; Sinisterra, R. D.; Cortés, M. E. Polycaprolactone Nanofibers Loaded Oxytetracycline Hydrochloride and Zinc Oxide for Treatment of Periodontal Disease. *Mater. Sci. Eng., C* **2019**, *103*, 109798.
(48) Palacios Hinestroza, H.; Urena-Saborio, H.; Zurita, F.; Guerrero de León, A. A.; Sundaram, G.; Sulbarán-Rangel, B. Nanocellulose and Polycaprolactone Nanospun Composite Membranes and Their Potential for the Removal of Pollutants from Water. *Molecules* **2020**, *25* (3), 683.
(49) Cervini, P.; MacHado, L. C. M.; Ferreira, A. P. G.; Ambrozini, B.; Cavalheiro, ÿ. T. G. Thermal Decomposition of Tetracycline and Chlortetracycline. *J. Anal. Appl. Pyrolysis* **2016**, *118*, 317−324.
(50) Fugita, R. A.; Gálico, D. A.; Guerra, R. B.; Perpétu, G. L.; Treu-Filho, O.; Galhiane, M. S.; Mendes, R. A.; Bannach, G. Thermal Behaviour of Curcumin. *Brazilian J. Therm. Anal.* **2012**, *01* (01), 19−23.
(51) Oliveira, J. E.; Mattoso, L. H. C.; Orts, W. J.; Medeiros, E. S. Structural and Morphological Characterization of Micro and Nanofibers Produced by Electrospinning and Solution Blow Spinning: A Comparative Study. *Adv. Mater. Sci. Eng.* **2013**, *2013*, 1−14.
(52) Zhou, X.; Ding, C.; Cheng, C.; Liu, S.; Duan, G.; Xu, W.; Liu, K.; Hou, H. Mechanical and Thermal Properties of Electrospun Polyimide/RGO Composite Nanofibers via in-Situ Polymerization and in-Situ Thermal Conversion. *Eur. Polym. J.* **2020**, *141*, 110083.
(53) dos Santos, D. M.; Leite, I. S.; Bukzem, A. d. L.; de Oliveira Santos, R. P.; Frollini, E.; Inada, N. M.; Campana-Filho, S. P. Nanostructured Electrospun Nonwovens of Poly(ε-Caprolactone)/Quaternized Chitosan for Potential Biomedical Applications. *Carbohydr. Polym.* **2018**, *186*, 110−121.
(54) Zupančič, Š.; Preem, L.; Kristl, J.; Putrinš, M.; Tenson, T.; Kocbek, P.; Kogermann, K. Impact of PCL Nanofiber Mat Structural Properties on Hydrophilic Drug Release and Antibacterial Activity on Periodontal Pathogens. *Eur. J. Pharm. Sci.* **2018**, *122*, 347−358.
(55) Church, D.; Elsayed, S.; Reid, O.; Winston, B.; Lindsay, R. Burn Wound Infections. *Clin. Microbiol. Rev.* **2006**, *19* (2), 403−434.
(56) Prado-Prone, G.; Silva-Bermudez, P.; Bazzar, M.; Focarete, M. L.; Rodil, S. E.; Vidal-Gutiérrez, X.; García-Macedo, J. A.; García-Pérez, V. I.; Velasquillo, C.; Almaguer-Flores, A. Antibacterial Composite Membranes of Polycaprolactone/Gelatin Loaded with Zinc Oxide Nanoparticles for Guided Tissue Regeneration. *Biomed. Mater.* **2020**, *15* (3), 035006.
(57) Yang, Y. N.; Lu, K. Y.; Wang, P.; Ho, Y. C.; Tsai, M. L.; Mi, F. L. Development of bacterial cellulose/chitin multi-nanofibers based smart films containing natural active microspheres and nanoparticles formed in situ. *Carbohydr. Polym.* **2020**, *228*, 115370.
(58) Bui, H. T.; Chung, O. H.; Dela Cruz, J.; Park, J. S. Fabrication and Characterization of Electrospun Curcumin-Loaded Polycaprolactone-Polyethylene Glycol Nanofibers for Enhanced Wound Healing. *Macromol. Res.* **2014**, *22* (12), 1288−1296.
(59) Azhdarzadeh, F.; Hojjati, M. Chemical Composition and Antimicrobial Activity of Leaf, Ripe and Unripe Peel of Bitter Orange (Citrus Aurantium) Essential Oils. *Nutr. Food Sci. Res.* **2016**, *3* (1), 43−50.
(60) Wormser, G. P.; Pakyz, A. L. Antibiotics Basics For Clinicians: Choosing the Right Antibacterial Agent Alan R. Hauser Philadelphia: Lippincott Williams & Wilkins, 2007 320 Pp., Illustrated. $32.95. *Clin. Infect. Dis.* **2008**, *46* (3), 485.
(61) Haroosh, H. J.; Dong, Y.; Lau, K.-T. Tetracycline Hydrochloride (TCH)-Loaded Drug Carrier Based on PLA:PCL Nanofibre Mats: Experimental Characterisation and Release Kinetics Modelling. *J. Mater. Sci.* **2014**, *49* (18), 6270−6281.
(62) Ahmad Wsoo, M.; Izwan Abd Razak, S.; Shahir, S.; Ahmed Abdullah Al-Moalemi, H.; Rafiq Abdul Kadir, M.; Hasraf Mat Nayan, N. Development of Prolonged Drug Delivery System Using Electrospun Cellulose Acetate/Polycaprolactone Nanofibers: Future Subcutaneous Implantation. *Polym. Adv. Technol.* **2021**, *32* (9), 3664−3678.
(63) Ullah, A.; Saito, Y.; Ullah, S.; Haider, M. K.; Nawaz, H.; Duy-Nam, P.; Kharaghani, D.; Kim, I. S. Bioactive Sambong Oil-Loaded Electrospun Cellulose Acetate Nanofibers: Preparation, Characterization, and in-Vitro Biocompatibility. *Int. J. Biol. Macromol.* **2021**, *166*, 1009−1021.
(64) Locilento, D. A.; Mercante, L. A.; Andre, R. S.; Mattoso, L. H. C.; Luna, G. L. F.; Brassolatti, P.; Anibal, F. d. F.; Correa, D. S. Biocompatible and Biodegradable Electrospun Nanofibrous Membranes Loaded with Grape Seed Extract for Wound Dressing Application. *J. Nanomater.* **2019**, *2019*, 1−11.
(65) Schneider, R.; Mercante, L. A.; Andre, R. S.; Brandão, H. d. M.; Mattoso, L. H. C.; Correa, D. S. Biocompatible Electrospun Nanofibers Containing Cloxacillin: Antibacterial Activity and Effect of PH on the Release Profile. *React. Funct. Polym.* **2018**, *132*, 26−35.
(66) Dias, G. C.; Cellet, T. S. P.; Santos, M. C.; Sanches, A. O.; Malmonge, L. F. PVDF Nanofibers Obtained by Solution Blow Spinning with Use of a Commercial Airbrush. *J. Polym. Res.* **2019**, *26* (4), 87.
(67) Hashmi, S.; Ahmed, R.; Rehman, A. U.; García-Peñas, A.; Zahoor, A.; Khan, F.; Vatankhah-Varnosfaderani, M.; Alshahrani, T.; Stadler, F. J. Study of the Synergistic Influence of Zwitterionic Interactions and Graphene Oxide on Water Diffusion Mechanism and Mechanical Properties in Hybrid Hydrogel Network. *Chemosphere* **2023**, *314*, 137710.
(68) International Organization for Standardization. *Tests for In Vitro Cytotoxicity*, 2009.

https://doi.org/10.1021/acsapm.4c00071
ACS Appl. Polym. Mater. 2024, 6, 5089−5101